Journal of Catalysis 428 (2023) 115177

Contents lists available at ScienceDirect

Journal of Catalysis

journal homepage: www.elsevier.com/locate/jcat

Research article

Structure-activity relationships of ZrO_2 crystalline phases in the catalytic transfer hydrogenation of methyl levulinate with ethanol

Riccardo Bacchiocchi [a,c,1], Alessia Ventimiglia [a,c,1], Andrea Canciani [a,c], Giorgia Peroni [a], Tommaso Tabanelli [a,c,*], Stefania Albonetti [a,c], Nikolaos Dimitratos [a,c], Ivan Rivalta [a,c,d,*], Shima Zainal [b], Luke Forster [b], Carmine D'Agostino [b,e,*], Fabrizio Cavani [a,c]

[a] Dipartimento di Chimica Industriale "Toso Montanari", Università di Bologna, Viale Risorgimento 4, 40136 Bologna, Italy
[b] Department of Chemical Engineering, School of Engineering, The University of Manchester, Oxford Road, Manchester M13 9PL, United Kingdom
[c] Center for Chemical Catalysis - C3, Alma Mater Studiorum Università di Bologna, Viale Risorgimento 4, 40136 Bologna, Italy
[d] ENSL, CNRS, Laboratoire de Chimie UMR 5182, 46 allée d'Italie, 69364 Lyon, France
[e] Dipartimento di Ingegneria Civile, Chimica, Ambientale e dei Materiali (DICAM), Alma Mater Studiorum – Università di Bologna, Via Terracini, 28, 40131 Bologna, Italy

ARTICLE INFO

Keywords:
H-transfer
Continuous-flow
γ-valerolactone
NMR relaxation
DFT calculation

ABSTRACT

The depletion of fossil resources is driving the research towards renewable alternatives, like lignocellulosic biomass. Therefore, the development of efficient continuous-flow processes, allowing to achieve better productivity compared to batch processes, will play a crucial role in promoting a sustainable transition. In this context, we report on the continuous-flow, gas-phase, catalytic transfer hydrogenation (CTH) of methyl levulinate and ethanol over zirconia catalysts, in particular focusing on the effect of two different crystalline phases (i.e. monoclinic, *m*-ZrO_2, and tetragonal, *t*-ZrO_2) on catalyst performance. An in-depth catalyst characterisation was coupled with both computational and ^{1}H NMR relaxation studies to assess the structure-activity relationship, providing fundamental insights into the catalytic process and future catalyst optimization. The results, indicate that the higher Lewis acidity and basicity along with the lower affinity with ethanol of *m*-ZrO_2 with respect to *t*-ZrO_2 are responsible for the promotion of undesired oligomerisation reactions of angelica lactones responsible for catalyst deactivation.

1. Introduction

Current world energy needs are largely supplied using fossil fuels (coal, oil and natural gas) leading to the progressive depletion of these sources and to the impactful emission of harmful greenhouse gases (GHG) such as: carbon dioxide (CO_2), methane (CH_4) and nitrous oxide (N_2O) [1-3]. Therefore, the potential use of renewable raw materials in place of fossil fuels has become a crucial area of research interest for the future of the chemical process industry. Plant-based raw materials (i.e. lignocellulosic biomass) have been suggested as fossil fuel alternatives for industrial production processes and for use as an energy source in the transport sector [4]. Moreover, the relative abundance and more uniform distribution of biomass across the planet imply that the incorporation of biomass into the industrial profile can help to achieve energy independence and develop new opportunities for the chemical industry.

The "Biomass Value-Added Chemicals" report published by the United States Department of Energy in 2004 [5] reported a list of twelve molecules derived primarily from renewable sources, listed along with their potential as biomass-based building block intermediates for the development of future biorefineries.

Among these molecules, levulinic acid (LA) and its esters (levulinic esters, LE) are particularly interesting at the industrial level. Indeed, LA can be obtained directly from cellulose by a cascade sequence of acid catalysed reactions namely: i) the hydrolysis of cellulose to glucose, ii) the subsequent isomerisation of glucose to fructose, iii) fructose

* Corresponding authors at: Dipartimento di Chimica Industriale "Toso Montanari", Università di Bologna, Viale Risorgimento 4, 40136 Bologna, Italy (T. Tabanelli and I. Rivalta). Department of Chemical Engineering, School of Engineering, The University of Manchester, Oxford Road, Manchester M13 9PL, United Kingdom (C. D'Agostino).
E-mail addresses: tommaso.tabanelli@unibo.it (T. Tabanelli), i.rivalta@unibo.it (I. Rivalta), carmine.dagostino@manchester.ac.uk (C. D'Agostino).
[1] These authors contributed equally to this work.

https://doi.org/10.1016/j.jcat.2023.115177
Received 3 June 2023; Received in revised form 13 October 2023; Accepted 19 October 2023
Available online 21 October 2023

dehydration to hydroxymethylfurfural (HMF) and finally iv) HMF hydration to an equimolar mixture of LA and formic acid [6]. Similarly, the acid-catalysed, direct alcoholysis of cellulose with light alcohols (e.g. methanol and ethanol) has recently been reported as an efficient strategy to obtain LE with good yield, thus lowering the formation of humins as by-products [7,8].

Thanks to the presence of both the ketonic and the carboxylic groups, LA and LE can be transformed to other, more useful molecules, through a range of chemical transformations including; hydrogenation, oxidation, amination, cyclisation and condensation reactions [9-13].

Among the various possible products obtainable from LA, γ-valerolactone (GVL) is of particular interest. In fact, it has many applications in various sectors such as a component in fragrance manufacture, a food additive, a bio-based solvent and as fuel additive (due to its high energetic power) [6,14]. Several processes have been proposed to obtain GVL from LA, employing both homogeneous and heterogeneous catalysis, mainly by promoting a hydrogenation reaction by using a high pressure of molecular hydrogen, in the liquid phase, under batch conditions. Phosphine complexes of transition metals, in particular Ru and Ir phosphine complexes, are particularly active as homogeneous catalysts [16]. Worth of note, the use of $[Ru(II)Cl_2(PPh_3)_3]$ complex, under optimised reaction conditions (180 °C, 12 bar of H_2), obtains GVL in almost quantitative yield (ca. 99%) but after 24 h of reaction in batch. Since LA is soluble in water, it is also possible to use water-soluble complexes, namely $[Cp^*Ir(H_2O)(4,4\text{-di-MeO-}2,2\text{-diPy})]SO_4$ or $Ru(acac)_3$ coupled with sulfonated triphenylphosphine ligands [15,16].

Although these processes are particularly selective with a high catalytic activity, they are difficult to apply on an industrial scale due to the inherent difficulty related to catalyst recovery, separation and recycling typical of homogeneous catalytic systems. Consequently, research has focused to the use of heterogeneous catalytic systems. For instance, a commercial 5% wt Ru/C in water or in a mixture of water and ethanol (temperature of 130 °C, H_2 at 12 bar, reaction time of 160 min), gives almost total conversion of LA (99.5%) and a selectivity to GVL of 86.6%. Moreover, addition of strongly acidic sulfonated resin (Amberlyst-70) mechanically mixed with 5% wt Ru/C, allows conversion of LA using milder conditions (5 bar H_2 and temperature of 70 °C) with similar results in terms of GVL yield [17]. Notably, recent improvements have led to development of the continuous-flow hydrogenation of LA or LE over fixed-bed, noble metal catalysts (i.e. Au supported over TiO_2, CeO_2 or Al_2O_3) [18], and non-noble metal catalysts (i.e. Cu/Al_2O_3, Ni/SiO_2 and Co/SiO_2) with promising results in term of GVL yield (between 67 and 86%) [19]; yield which become close to 100% when innovative reactors based on microwaves and Ru/TiO_2 are employed [20]. However, the use of high hydrogen pressures can lead to major safety problems and high plant maintenance costs. Furthermore, the need for noble metal-based catalysts to facilitate the activation of molecular hydrogen may result in major environmental and economic issues. Therefore, research focused on developing catalysts utilising cheaper, more accessible and readily available metals.

In recent years, alternative reaction routes based on Catalytic Transfer Hydrogenation (CTH) *via* the Meerwein-Ponndorf-Verley (MPV) mechanism have been reported, where small molecules (i.e. light alcohols) are used as reducing agents (H-donor) for bio-based platform chemicals [21-27]. In particular, the use of zirconium oxide (ZrO_2), also called zirconia, has been widely demonstrated to be an excellent catalyst for CTH reactions, particularly that of LA and LE, since the inspiring works of Dumesic et al. [28] owing to its amphiphilic nature with the presence of both Lewis acid and basic sites and high-temperature resistance. In particular, the fine tuning of both acid and basic sites strength and density over the catalyst surface play a crucial role in the synergetic activation of both the H-donor and the reducible substrates, thus fostering a rapid and efficient H-transfer *via* the MPV mechanism [21,29]. Nonetheless, considering the current available literature on the CTH of LA or LE with alcohols, the great majority of the works are related to the application of ZrO_2 based catalysts in batch, liquid-phase setups, in which the H-donor (often secondary alcohols like isopropanol or 2-butanol) is often used in large excess, behaving both as a reagent and the reaction solvent. In some cases this approach may lead to good results in terms of GVL yield (91–96%) but often the reaction requires several hours (8–10 h) to achieve high LA conversion [30-32]. In 2019, we firstly reported on the possibility to perform the CTH of LE with ethanol (and bio-ethanol) or other alcohols in a continuous-flow, gas-phase, fixed bed reactor [33,34]. In this way, the advantages of this approach were demonstrated, allowing the use of a wide range of reaction temperatures (i.e. from the boiling point of the mixtures up to 500 °C) at atmospheric pressure, making the process safer, more productive and convenient compared to analogous tests performed in batch and liquid phase. Due to their lower boiling points and higher stabilities at high temperatures, LE, methyl levulinate (ML) and ethyl levulinate (EL) were preferred to LA as reducible substrates for the gas phase approach. Interestingly, the use of a relatively high surface area tetragonal zirconia catalyst (*t*-ZrO_2, SSA: 120 m^2/g) gave promising results using ethanol as H-donor. Under optimized reaction conditions (contact time of 1 s, 250 °C), it was possible to reach total ML conversion and a GVL yield of around 70%. A possible reaction scheme was also proposed using the results of dedicated tests (see Scheme 1) [33]. The commonly accepted mechanism reported for the liquid phase reduction of LA/LE, consists of the reduction of the carbonyl group leading to the formation of the highly reactive 4-hydroxypentanoic acid (or ester). Conversely, the gas-phase reduction of LA/LE over ZrO_2 leads to the fast, efficient, intramolecular cyclisation of LE to angelica lactones (α/β AL). These compounds are key intermediates that may then undergo the consecutive CTH with EtOH thereby yielding GVL. It follows that, the hypothesised reaction scheme based on the CTH of AL to GVL is not a rigorous MPV concerted mechanism over the catalytic surface with the formation of a six-membered intermediate between the carbonyl containing substrate, the alcohol used as H-donor and the catalyst' surface. Nonetheless, the actual mechanism should follow a "MPV-like pathway" in which the carbonyl of the lactone ring can interact with the Lewis acid sites over the catalyst surface in a similar way compared to the traditional mechanism, this way favouring the CTH reduction of the vicinal double bond. Ethyl γ-valerolactone (Ethyl GVL) is most likely formed by means of the parallel hydroxyethylation of ALs by acetaldehyde (co-produced by the H-transfer of EtOH) and the dehydration and reduction of the C-OH moiety. Moreover, acid sites on the catalyst can promote GVL ring-opening and the consecutive dehydration reaction to form ethyl pentenoates (EP). In spite of the very interesting results obtained by working with ethanol as H-donor for the production of GVL in the gas-phase, a progressive deactivation of the ZrO_2 catalyst has been observed. This is due to the deposition of heavy carbonaceous residue over most of the Lewis acid sites which are crucial for the CTH process, leading to a progressively promotion of parasite alcoholysis and transesterification reactions (i.e. increased ethyl levulinate (EL) formation via ALs alcoholysis) [33]. The observed catalyst fouling was hypothesised to be mainly due to AL and/or acetaldehyde oligomerization but not further investigated in depth nor linked to specific acid or basic catalysis.

It is clear that the beneficial properties of zirconia make it a very interesting material for the CTH of LA/LE to produce GVL. Additionally, it has the significant advantages of being very cheap and readily available in three different crystalline forms: monoclinic, tetragonal and cubic. Among them, the monoclinic (*m*-ZrO_2) and tetragonal (*t*-ZrO_2) are most investigated and applied crystalline phase of ZrO_2 in catalysis due to the higher specific surface area achievable on the respect of the cubic form and different properties. Indeed, these two zirconia phases possess differing symmetry and a differing coordination of the exposed atoms over the ZrO_2 surface. In particular, the distinct atom conformation in *t*-ZrO_2 leads to octa-coordinated Zr^{4+} cations with tetra-coordinated O^{2-} anions (symmetry $P4_2/nmc$) while in *m*-ZrO_2, the Zr^{4+} cations are hepta-coordinated and the O^{2-} anions are tri- or tetra-coordinated (symmetry $P2_1/c$). Such diverse structural arrangements lead to different types of

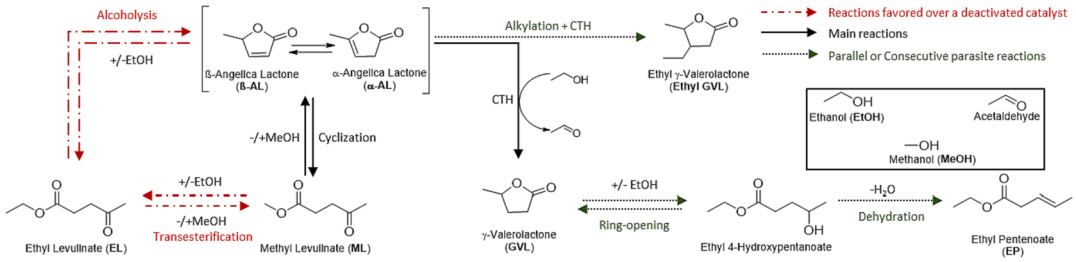

Scheme 1. Simplified reaction pathways for the CTH of ML with EtOH toward GVL and the main by-products.

coordinatively unsaturated surface sites and will consequently lead to peculiar acid-base surface properties [35,36].

For all these reasons, an in-depth investigation and comparison of these two different crystalline phase zirconia catalysts with a similar specific surface area, namely, a tetragonal and a monoclinic zirconia catalyst (*t*-ZrO_2 and *m*-ZrO_2 respectively), is herein reported. In particular, this work by using catalytic, computational and NMR relaxation studies is aimed to address a structure-activity relationship between the surface properties of these two different ZrO_2 polymorphs and the catalytic activity shown for the CTH of ML with ethanol, with the final goal not only to further increase GVL yield but also to understand how to further optimise future catalysts design to strongly increase catalyst lifetime (i.e. by limiting parasite AL oligomerisation reactions over the surface) in order to make this alternative strategy actually competitive and sustainable.

2. Experimental

2.1. Synthesis of ZrO_2–based catalysts

Tetragonal Zirconia (t-ZrO_2) catalyst was prepared by the precipitation methodology proposed by Chuah [37]. An aqueous solution of ZrO$(NO_3)_2{\cdot}2H_2O$ (0.3 M) was added dropwise to a stirred aqueous solution of NH_4OH (5 M) at room temperature. Afterwards, the solution was digested at 100 °C for 24 or 48 h under reflux. The pH of the solution was adjusted to 9 during the digestion by the continuous addition of 5 M NH_4OH though an high precision infusion pump (KDScientific Legacy Syringe-infusion Pump) setting up a flow of 2.9 mL/h. The precipitate was separated by filtration and washed with 1 L of NH_4OH aqueous solution (5 M) for 10 g of catalyst. After the filtration step, the sample was dried at 100 °C overnight and then calcined in air at 500 °C for 12 h with a heating rate of 5 °C/min.

Monoclinic Zirconia (m-ZrO_2) catalyst was prepared by hydrothermal synthesis. An aqueous solution was prepared by adding 3.38 g of ZrO$(NO_3)_2{\cdot}2H_2O$ to 20 mL of distilled water. Afterwards, 6.06 g of urea were added, and the solution was then transferred to an autoclave with a Teflon inlet. The autoclave was placed inside a furnace with a temperature of 140 °C for 20 h. Afterwards, the precipitate was centrifuged with ethanol and then with distilled water. Finally, the sample was dried at 100 °C overnight and then calcined in air at 450 °C for 3 h with a heating rate of 5 °C/min.

2.2. Catalysts characterisation

X-ray powder diffraction (XRD) patterns were collected with a Ni-filtered Cu Kα radiation (λ = 1.54178 Å) on a Philips X'Pert vertical diffractometer equipped with a pulse height analyser and a secondary curved graphite-crystal monochromator.

BET specific surface area of the catalysts was determined by N_2 absorption–desorption at −196 °C using a Sorpty 1750 Fison instrument. 0.1 g of the sample was used for the measurement, and the sample was outgassed at 150 °C before N_2 absorption.

NH_3-CO_2-temperature-programmed desorption (TPD) measurements were collected with a Autochem TPD/R/O 2920 automated system for analysing the acid/base properties of catalysts. Fresh catalyst was pretreated in 10 vol% O_2 in He (30 mL/min of flow rate) at 500 °C for 1 h following a heating ramp of 10 °C/min to remove adsorbed H_2O and CO_2. The catalyst was then exposed to the probe molecule for 1 h with a flow of 30 mL/min of 10 vol.0% of NH_3 or CO_2 in He. Physisorbed molecules were removed by flushing with He (30 mL/min of He) for 10 min prior to analysis. Finally, the temperature-programmed desorption was performed following the desorption with both TCD and MS, increasing the temperature with a heating rate of 10 °C/min from 40/100 °C to 450 °C in He (30 mL/min).

Thermogravimetric/differential thermal analyses (TGA/DTA) were performed using a SDT Q 600 instrument, TG/DT analyses were performed using fresh and spent catalysts. Typically, 100 mg of the sample was used for the measurement at temperatures ranging from room temperature to 700 °C, with a heating rate of 10 °C/min in air.

In Situ Diffuse Reflectance Infrared Fourier Transform Spectroscopy (DRIFT) of dimethyl pyridine (DMP) were performed in order to characterised and distinguish between Lewis and Brønsted acid sites. Typically, a ZrO_2 sample was loaded in the cell and pretreated at 400 °C under a flow of He (10 mL/min) for 60 min in order to clean the surface and remove any adsorbed molecules. Then, using KBr as the background, spectra were acquired every 50 °C in range 50–400 °C. Next, a pulse of DMP (2 μL) was introduced over the sample at 50 °C. IR spectra were then acquired at 1 min time intervals to follow the adsorption process. For the desorption process, the sample was heated up to 400 °C (heating rate of 5 °C/min) and spectra were acquired every 50 °C up to 400 °C. DRIFT spectra were acquired in situ with a Bruker Vertex 70 instrument equipped with a Pike DiffusIR cell attachment. Spectra were recorded using an MCT detector after 128 scans and with a 4 cm^{-1} resolution in the region of 4000–450 cm^{-1}.

Energy dispersive spectrometry (EDS) was carried out with a scanning electron microscope (SEM) Zeiss EP EVO 50 equipped with an INCA X-Act penta FET Precision detector (Oxford Instruments Analytical). Spectra were recorded with an accelerating voltage of 20 kV for 60 s.

2.3. Catalytic tests

CTH tests were carried out by the vaporisation of an alcohol/levulinate ester (molar ratio 10:1, liquid flow was 0.5 mL/h in a N_2 stream). The liquid mixture was fed by means of a syringe pump (KDScientific Legacy Syringe-infusion Pump) into a stainless-steel heated line to allow for instant vaporisation. An inlet with the carrier gas (N_2) arrives to this line, and then this line is connected to a tubular glass reactor (length 450 mm, inner diameter 19 mm) containing 1 cm^3 of catalyst with the desired particle size (i.e. 30–60 mesh). Generally, the residence time for the catalytic tests was 1 s and the %mol of the organic mixture was fixed between 8 and 12%. The reactor was placed inside a furnace and its inlet and outlet were covered with heating tapes equipped with an electrical resistance to regulate the inlet and outlet temperature. Before every CTH test, the catalyst was pre-treated inside the reactor for 2 h at 400 °C using 30 mL/min air flow. Afterwards, the temperature of both the furnace and heating tape was set to the desired temperature (normally

250 °C and 230 °C, respectively). During the CTH tests, the exit stream was condensed using a cold trap filled with 25 mL of acetonitrile in order to collect the heavier products of the reaction. The collected acetonitrile solution was taken and analysed every 50–60 min to monitor the reactivity during the time-on-stream process.

Reaction products were analysed and quantified using a Thermo Focus GC gas-chromatograph equipped with a non-polar capillary column Agilent HP-5 (5% phenyl–95% methylsiloxane) as reported in detail in the supporting information section S2.

Knowing the molar flow rate of the reactants (expressed in mol/min) and the collection time, the product yields (Y) and the conversion (X) of the reagent were calculated with as follow:

$$X_{reactant} = \frac{mol^{in}_{reactant} - mol^{out}_{reactant}}{mol^{in}_{reactant}} * 100$$

$$Yproduct = \frac{mol^{out}_{product}}{mol^{in}_{reactant}} * 100$$

In addition, carbon balance based on alkyl levulinate was considered as follows:

$$\frac{Y}{C} = \frac{\Sigma products \;\; yield}{Reactant \;\; conversion} *100$$

2.4. ^1H NMR relaxation measurements

All NMR relaxation measurements were carried out using a Magritek Spinsolve benchtop NMR spectrometer operating at a ^1H frequency of 43 MHz. NMR measurements were performed at STP (25 °C, 1 atm). The typical relative error for all NMR relaxation measurements was approximately 3 %.

2.4.1. 1D T_1 and T_2 NMR relaxation measurements

Monoclinic and tetragonal ZrO_2 particles were soaked in either *n*-octane, methanol, ethanol, ML, EL, α-AL and GVL for 24 h prior to analysis. The ZrO_2 particles were then removed from the respective liquid and gently dried on a pre-soaked filter paper to remove excess liquid from the outer surface whilst avoiding removal of liquid from the internal pore structure. Following drying, the ZrO_2 particles were transferred to 5 mm NMR tubes and the tube was finally placed into the magnet and left for approximately 15 min before starting the measurements, in order to achieve thermal equilibrium.

T_1 spin–lattice relaxation times were measured using an inversion recovery pulse sequence (Fig. 1a), [38] with sixteen recovery delays (in the range 1 ms−5000 ms) logarithmically spaced and 8 scans per step. The maximum delay and repetition time was set equal to ~5 × T_1.

The T_2 spin-spin relaxation times were measured using the Carr-Purcell-Meiboom-Gill (CPMG) sequence, (Fig. 1b) [39] with an echo time of 120 μs and range of 50 to 500 echoes per step. 16 logarithmically spaced steps were used with 8 scans per step. The repetition time was set equal to ~5 × T_1.

2.5. Computational methods

The nanoparticulate structures of the two crystalline phases of ZrO_2 were modelled according to the cluster approach. In fact, the main aim of the computational work was to analyse the behaviour of the different catalytic sites locally present on the nanoparticle surfaces of each phase. Although Brønsted sites could play a role in MPV reactions [40], considering the pretreatment of the catalyst at 400 °C prior each reactions and since the number of Brønsted sites can vary due to a dissociative adsorption of water,[41] we decided to carry out a computational study that was independent from the reaction conditions, i.e. neglecting models the OH covered NPs, to simply evaluate the interactions of the target molecules on the surface of the catalysts. The geometry optimisations have been performed in vacuum at the Density Functional Theory (DFT) level, using the B3LYP exchange-correlation functional, [42] as implemented in the *Gaussian 16* package [43]. Adsorption studies of CO_2, NH_3 and α-AL have been performed on top of optimised ZrO_2 structures for both crystalline phases. For geometry optimizations, the 6-31G** basis set [44-48] was used for light atoms (H, C and O) while the Stuttgart effective core potential has been employed for the Zr atoms [49]. The adsorption energies have been computed on top of optimised geometries with a larger basis set, i.e. 6-311++G**, for H, C and O. In order to account for the basis set superposition error (BSSE), the counterpoise correction was applied, as implemented in the *Gaussian 16* package [50,51]. The adsorption energy (AE) of the adsorbate (ads) on the nanoparticles (NP) was computed as:

$$AE = E_{NP+ads} - (E_{NP} + E_{ads})$$

3. Results and discussion

3.1. Characterisation of t-ZrO_2 and m-ZrO_2 catalysts

Two different ZrO_2 catalysts were synthesised following and optimising two alternative synthetic strategies already reported in literature, namely a precipitation in a controlled environment and a hydrothermal

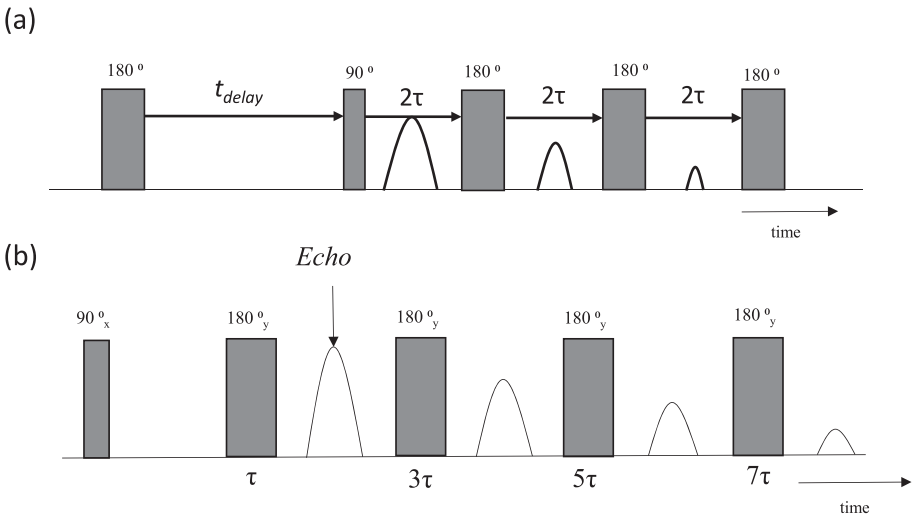

Fig. 1. (a) Inversion recovery pulse sequence and (b) CPMG pulse sequence. The thin and thick vertical bars represent 90° and 180° radiofrequency (RF) pulses, respectively.

synthesis [37,52]. These strategies were implemented and optimised to produce two different crystalline phases: a high purity tetragonal and a pure monoclinic phase (Fig. 2a), characterised by a relatively high, yet similar, specific surface areas of 120 and 117 m^2/g for *t*- and *m*-ZrO_2 respectively. *t*-ZrO_2 was also characterised by means of SEM-EDX (see Table S1 in the supporting information) this way confirming the presence of traces of both Hf and Si, the former being a common impurity in several zirconia precursors that is difficult and expensive to separate because of its chemical similarity to zirconium [53]; while the latter (Si content in the sample equal to 0.5 %wt) could be related to a limited dissolution of SiO_2 from laboratory glassware, during the digestion at basic pH as already reported by Min et al. [54]. Even though this amount is among the lowest reported by Min et al. for impure zirconia, nevertheless we cannot exclude that the phenomena associated to the higher stability and higher surface area of the sample can be attributed to an effect of Si impurities. These improved properties may also affect the catalytic performances of the sample, while a direct role of Si as an active can be reasonably excluded because of its very low amount in our sample.

NH_3– and CO_2-TPD analysis of the fresh catalysts highlights the bifunctional properties of ZrO_2 proving the presence of both acidic and basic sites (Fig. 2b and 2c). *t*-ZrO_2 presents a single TPD peak centred at around 125 °C for CO_2, indicating the presence of only weak basic sites. Furthermore, the ammonia desorption profile shows a wide desorption peak from 150 °C to 450 °C, indicating the coexistence of weak, moderate and strong acid sites. On the other hand, *m*-ZrO_2, shows a similar NH_3 desorption profile however slightly shifted toward higher temperature and intensity, indicating a higher density of the strongest acid sites over the surface of this polymorph compared to *t*-ZrO_2. However, considering the *m*-ZrO_2 TPD profile of CO_2, the desorption peak area is roughly 4 times greater than the tetragonal analogue, with the maximum desorption temperature shifted to 145 °C, indicating the presence of a higher amount of stronger basic sites (Table 1). These differences between the two crystalline phases of ZrO_2 are in good accordance with the literature, [36] potentially playing a crucial role in promoting the selective CTH of ML with ethanol or in fostering parasite oligomerisation reactions leading to catalyst fouling.

Finally, dimethylpyridine DRIFT adsorption/desorption tests have been performed in order to assess the nature of the surface acidic sites (Figure S1). Dimethylpyridine (DMP, pKa of 6.6) was preferred to pyridine because the latter is known to be inefficiently protonated (or form H-bonds) with ZrO_2 weak Brønsted sites, while the former shows weaker affinity for Lewis acid sites due to the steric hindrance induced by the two methyl groups [55]. The adsorption spectra of DMP, recorded at 50 °C, highlight the predominant presence of Lewis acid sites in both the zirconia phases, demonstrated by the presence of the main bands centred at 1600, 1580 and at around 1470 cm^{-1}, which correspond to ν_{8a}, ν_{8b} and ν_{19a} DMP vibration modes, respectively. However, in both samples a negative band related to surface –OH groups consumption can be clearly seen at around 3700 cm^{-1} (not shown in Figure S1). This behaviour clearly indicates the titration of Brønsted sites. Interestingly, only for *t*-ZrO_2 few bands centred at 1473, 1640 and 1650 cm^{-1} corresponding to protonated DMP can be observed, nonetheless for this sample all the bands completely disappear up to 400 °C. On the contrary, in the case of *m*-ZrO_2, no bands of protonated DMP have been clearly detected. Nonetheless, a progressive shift of the main band at 1600 cm^{-1} to higher wavenumber can be observed, suggesting the presence of both coordinated (over Lewis acid sites) and H-bonded DMP (over Brønsted sites) [56]. Noteworthy, to completely desorb all the adsorbed DMP, a further increase to 450 °C is needed for *m*-ZrO_2 again highlighting the presence of stronger sites over this material.

Table 1
Crystalline nature, specific surface areas and acid-basic densities of ZrO_2 catalysts.

ZrO_2 Crystalline Phase (XRD)	SSA (m^2/g)	Acid density (µmol/m^2)	NH_3 T_{max} desorption (°C)	Basic density (µmol/m^2)	CO_2 T_{max} desorption (°C)
Tetragonal	120	4.08	Wide band from 150 °C to 450 °C	1.18	125 °C
Monoclinic	117	4.25	Wide band from 170 °C to 450 °C	4.97	Wide band from 130 °C to 350 °C

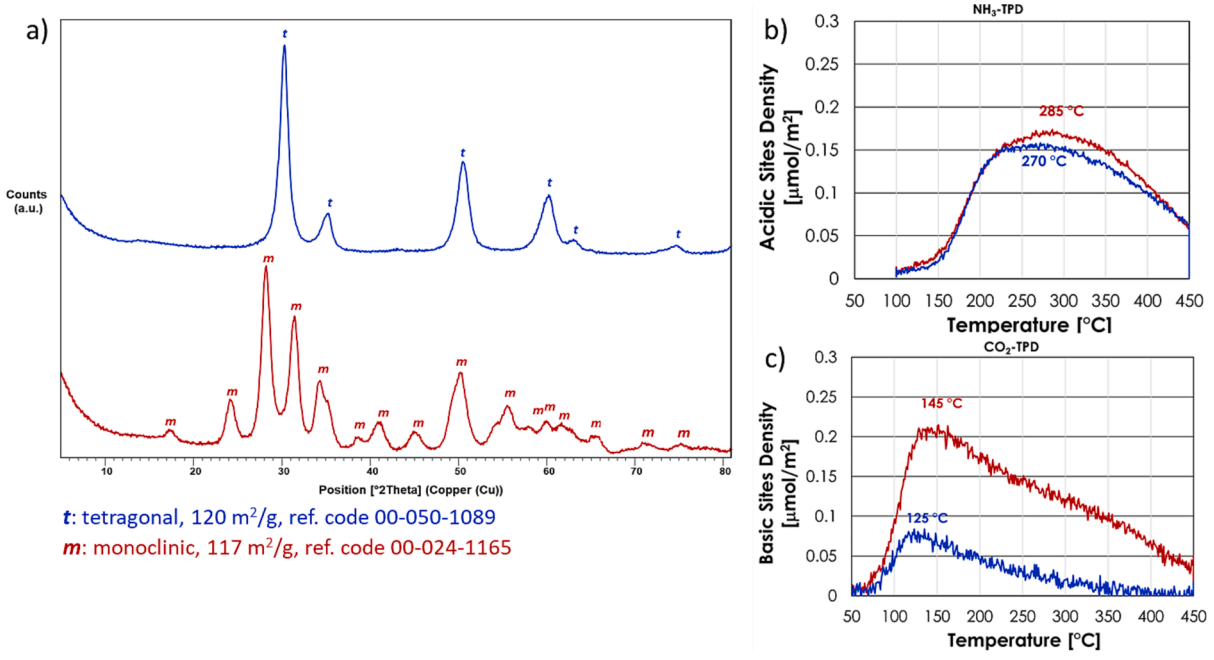

Fig. 2. a) XRD analysis of synthesised *t*-ZrO_2 (blue) and *m*-ZrO_2 (red); b) NH_3- and c) CO_2-TPD profiles of *t*-ZrO_2 (blue) and *m*-ZrO_2 (red). (For interpretation of the references to colour in this figure legend, the reader is referred to the web version of this article.)

3.2. Influence of ZrO_2 phases on CTH of ML with ethanol

Our previously reported studies focused on proving the feasibility of the CTH process of ML and ethanol in a continuous-flow, gas-phase reactor over *t*-ZrO_2 (Figure S2 in the Supporting Information) [33]. Here, new efforts have been made in order to investigate the catalytic activity of *m*-ZrO_2 in the same conditions, this way comparing and analysing in depth the effect of the crystalline phase on catalysts properties and activity. In particular, *m*-ZrO_2 was firstly investigated by feeding ML and EtOH, at 250 °C and a contact time of 1 s (Fig. 3).

Initially, the use of *m*-ZrO_2 allows to reach complete conversion of ML with a GVL yield of 63 %. Acetaldehyde is the co-product of CTH and it can act as a hydroxy-alkylating agent for ALs (α- and β-AL) thereby yielding a hydroxy-intermediate, which rapidly dehydrates and can be reduced via CTH to ethyl-GVL, which is the main by-product over the fresh catalyst at the beginning of the test (up to 200 min on stream). Ethyl-GVL could also, in principle, form by the alkylation of GVL but further tests ruled out this hypothesis, as discussed below. Noteworthy, there is very little in literature about ethyl-GVL. Nonetheless, Dupont in 2005 filed a patent in which substituted GVL are produced through a multistep sequence of reactions, starting from the condensation of a lactone with an oxalic acid diester. Interestingly, they claimed the use of these substituted GVL in fragrance and detergent formulation as well as promoters for enhancing the properties (e.g. rheology) of an oil, hydrocarbon or petroleum products [57]. Therefore, the properties of ethyl-GVL are worth of future investigations. Coming back to our catalytic results, after 200 min on stream, ML conversion starts to decline with a simultaneous, significant change of the chemoselectivity of the reaction that shifts from the selective formation of GVL toward the formation of EL. This behaviour is quite similar to the one obtained over *t*-ZrO_2 in the same reaction conditions (Figure S2). However, in the *m*-ZrO_2 case, it is strongly accelerated. As a matter of fact, the worse molar balance obtained over *m*-ZrO_2 (average $\sum$Y/X of 80% *vs* 94% over *t*-ZrO_2) clearly proves that a progressive and extensive deactivation is occurring due to the deposition of heavy carbonaceous residues on specific active sites of the catalytic surface. Moreover, over a deactivated catalyst, ALs were produced in small quantities (ca. 7% yield), suggesting that the deactivation is mainly affecting the consecutive CTH process between ethanol and ALs, with the latter formed *via* an intramolecular cyclization of ML. Therefore, the possibility of another reaction mechanism involving the reduction of the ketonic group can be disregarded, as previously suggested [33]. While the experimental evidences for *m*-ZrO_2 and *t*-ZrO_2 feature some similarities (see Figure S2), some crucial differences can be underlined: i) maximum GVL yield reached a value of about 73% over *t*-ZrO_2 and it maintains between 60 and 70% for around 320 min on stream; ii) better molar balances are obtained throughout the duration of the test on *t*-ZrO_2, proving both the greater stability and lower tendency of accumulating heavy compound with respect to *m*-ZrO_2.

At this point, the outcome suggests that the lower catalytic performance observed for *m*-ZrO_2 may be due either to the much higher density and strength of Lewis basic sites compared to the tetragonal form or to the slightly higher acidity observed in both TPD (see Table 1) and DRIFT experiments. Noteworthy, the stronger Lewis basicity may not only promote ALs formation, but also foster their oligomerisation over the catalyst surface, as previously observed in the case of stronger acidity leading to the formation of polymers containing carboxylic groups [58].

To further clarify the effect of the zirconia crystalline phase on the CTH activity, experiments were performed at different reaction temperatures and coupled with TGA analyses of the spent zirconia catalysts. Fig. 4 presents a summary of the main results concerning ML conversion (outer ring) and product yields (inner ring) performed at different reaction temperatures in the range 200–300 °C.

Table 2 compares the catalytic performances of *m*-ZrO_2 and *t*-ZrO_2 in terms of weight loss, desorption temperature and accumulation rate of heavy compounds over the spent catalytic materials, as determined by TGA (see details in Figure S3 in the SI).

Considering the results obtained from TGA analyses, the average rate of accumulation of organic compounds over the surface is always higher in the case of *m*-ZrO_2 compared to *t*-ZrO_2, independently from the reaction temperature.

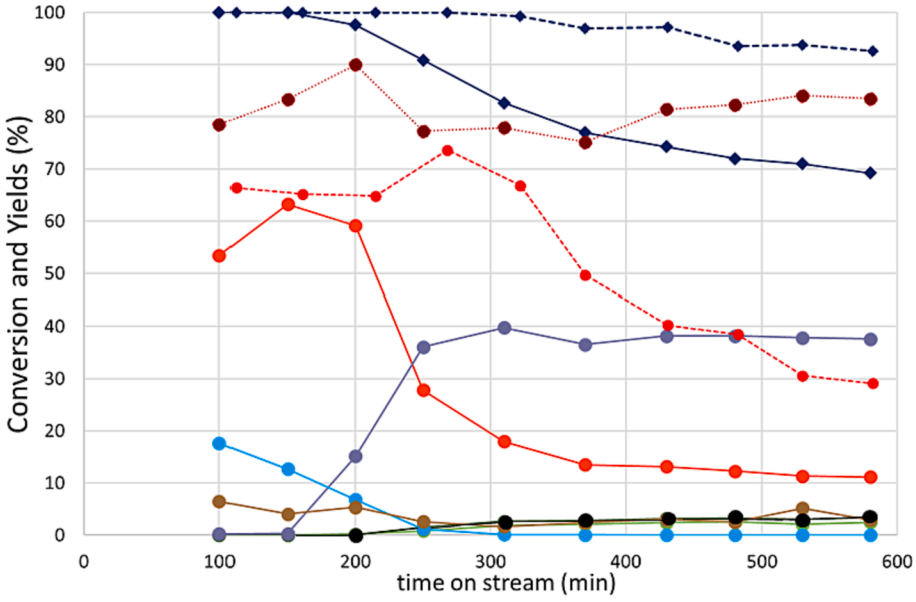

Fig. 3. Catalytic results obtained in ML reduction *via* CTH using EtOH as H-donor over *m*-ZrO_2. Reaction conditions: molar ratio ML:EtOH = 1:10, T = 250 °C, τ = 1 s, %mol N_2:ML:EtOH = 90.1:0.9:9. ML conversion (◆); EL (●); GVL (●); Ethyl GVL (●); αAL (●); βAL (●); Others (●); Yields sum/Conversion (● dotted line). For the sake of comparison the results obtained over *t*-ZrO_2 are also reported with dashed line in terms of both ML conversion (◆) and GVL yield (●).

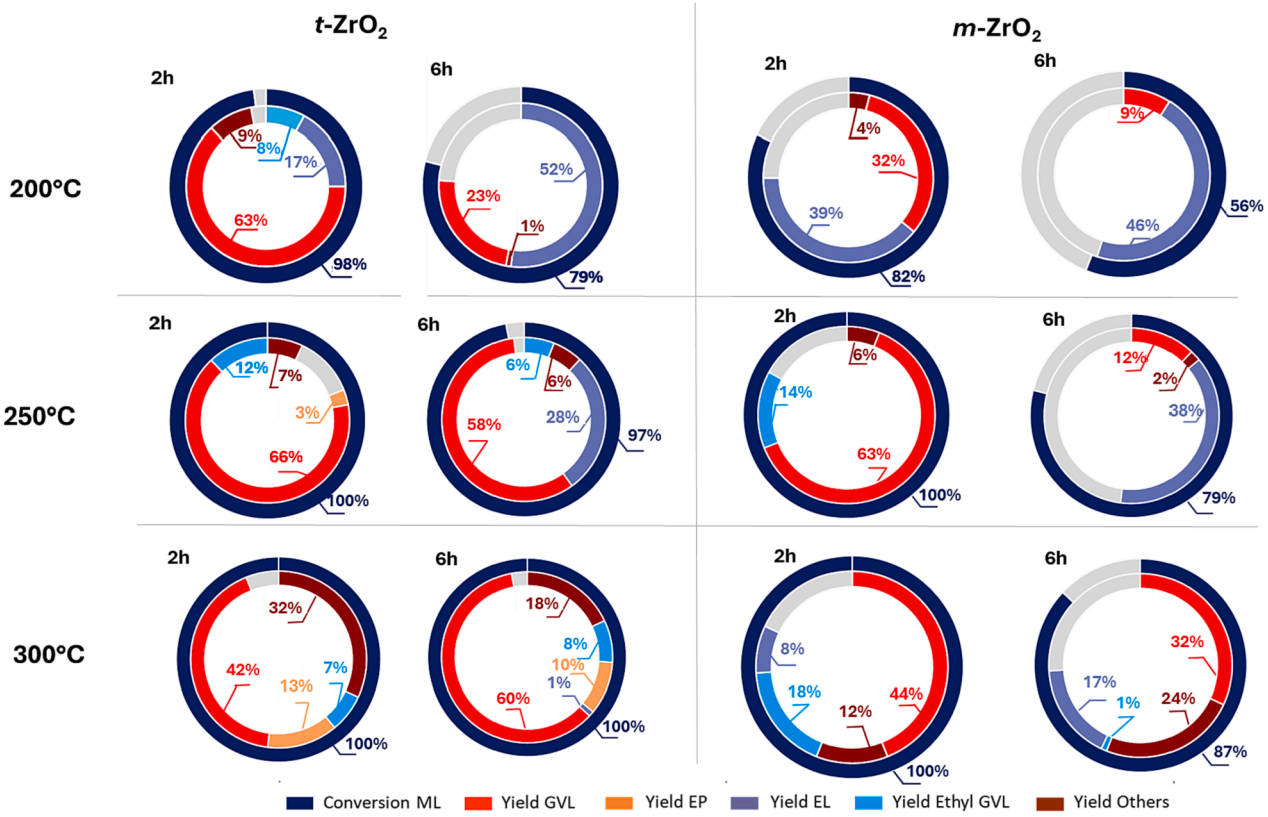

Fig. 4. Catalytic results obtained in ML reduction via CTH using EtOH as H-donor over both *m*-ZrO_2 and *t*-ZrO_2 phases. Reaction conditions: molar ratio ML:EtOH = 1:10, T = variable, τ = 1 s, %mol N_2:ML:EtOH = 90.1:0.9:9. Results related to 2 and 6 h on stream.

Table 2
Accumulation of heavy compounds obtained from TGA over spent ZrO_2 catalysts. Average accumulation rates are calculated by dividing the overall weight loss for the actual time on stream.

$T_{reaction}$ (°C)	Spent catalyst (m)	Weight loss (%)	Desorption T (°C)	Time on stream (min)	Accumulation rate (mg/h)
200	*t*-ZrO_2 (0.977 g)	5.89	326	548	6.3
	m-ZrO_2 (1.22 g)	5.35	315	592	6.6
250	*t*-ZrO_2 (1.08 g)	5.48	328	640	5.5
	m-ZrO_2 (1.18 g)	5.80	320	580	7.1
300	*t*-ZrO_2 (0.982 g)	6.30	349	605	6.1
	m-ZrO_2 (1.14 g)	6.57	338	592	7.6

Going into details and considering the catalytic results as a function of reaction temperature, at 200 °C both catalysts showed a rapid decrease in conversion with a systematic variation of chemoselectivity (see also Figure S4 in the SI), which is even more pronounced in the case of *m*-ZrO_2. The average accumulation rate of heavy organic compounds over the catalytic surface is comparable between both samples (between 6.3 and 6.6 mg/h), despite the relatively good molar balance of ML (expressed as $\sum Y/X$, as mentioned above). Probably, this relatively low reaction temperature is insufficient for effectively promote the CTH reactions, while the unselective oligomerisation of AL or acetaldehyde over the surface rapidly prevail leading to catalyst deactivation.

At 250 °C, a significant difference in terms of organic accumulation values between the two catalytic systems was observed, with *t*-ZrO_2 showing the lowest accumulation of heavy compounds among all the tests. This slower accumulation of heavy compounds over the catalyst was also proved by the improved results in terms of GVL yield (which is above 65% for the first 6 h of reaction, see Figure S2 in the SI). Interestingly, the accumulation of organic compounds over *m*-ZrO_2 seems to be only slightly affected by the reaction temperature and steadily increased in the range of 200 °C – 300 °C (Table 2).

At 300 °C (Figure S5, SI), both catalysts initially promoted consecutive reactions to ethyl-GVL and other by-products, showing a lower maximum of GVL yield values compared to 250 °C. However, while *t*-ZrO_2 produced significant amounts of ethyl pentenoates (EP), proving its ability to foster consecutive reactions like GVL ring-opening and dehydration reactions strongly limiting the formation of EL, *m*-ZrO_2 yields EL already after 2 h (reaching 20% yield after 6 h) and led to lower molar balances and to a progressive decrease in ML conversion. Moreover, in these experimental conditions, *t*-ZrO_2 showed a slow deactivation, proved by the progressive decrease of GVL consecutive products yields, slowly favoring GVL formation (with yield up to 60%) without any effect on the ML conversion (which is complete for almost 10 h on stream).

Taking into consideration the above catalytic results, it seems that at 200 °C the crystalline phase of the catalyst has a much lower influence upon the distribution of products, probably due to an inefficient activation of the CTH reactions, increasing the amount of available AL for oligomerisation leading to a fast catalyst deactivation in both cases. At intermediate reaction temperatures, the two catalysts showed significantly different catalytic behaviours in terms of heavy compounds accumulation rate and, as a consequence, deactivation rate and distribution of products. At 250 °C, the tetragonal phase significantly increased its resistance to adsorb heavy compounds on its surface, lowering the accumulation over time. However, this was found to be insufficient to keep the catalyst stable for several hours of reaction, finally leading to EL production. Increasing the reaction temperature to 300 °C led to an increase in accumulated compounds for both samples.

However, for the *m*-ZrO_2 a higher increase of the accumulate compounds was observed, most likely due to side reactions including decarboxylation to butenes and oligomerization of unsaturated compounds (including ALs). To better understand the role of ALs in both the CTH toward GVL and deactivation of the ZrO_2 catalysts, tests were performed feeding a mixture of α-AL and ethanol (1:10 M ratio) at 250 °C over *m*-ZrO_2, as shown in Fig. 5.

Interestingly, the obtained results showed similar trends compared to those reported in Fig. 1, again strongly suggesting the role of ALs as both primary product obtained through the ML cyclisation and key reaction intermediates. Moreover, in none of all the catalytic tests performed so far we ever observed the presence of hydroxypentanoate esters, neither in traces. Unfortunately, this compound is not available from the most common commercial suppliers so is not trivial to perform a comparison test; nonetheless, although we cannot completely rule out the formation of hydroxypentanoate esters, we thought to have enough experimental indication to address to AL a major role in the production of GVL and consecutive products in our gas-phase and continuous-flow process. Going into detail of the results showed in Fig. 5, for a period of 2 h of reaction, α-AL was completely converted, yielding mainly GVL (56 %) and ethyl GVL (11 %). Then, the same change in the chemoselectivity of the process discussed above was observed: GVL yield decreased significantly favouring the formation of both EL, strongly suggesting that EL is mainly formed by ALs alcoholysis and β-AL obtained via isomerisation processes. On the other hand, while feeding ML, only over a progressively deactivated catalyst the very reactive intermediate ALs can be observed due to the fast conversion of ML to ALs and then of ALs toward EL, GVL or heavy compounds (this being the reason why ALs yields are increasing with the time on stream). As seen also for *t*-ZrO_2 (see Figure S6 in the SI), these results strongly support the hypothesis that ALs are the key intermediates in the gas-phase CTH of ML with ethanol and that ZrO_2 is able to promote the effective and rapid cyclisation of ML. On the other hand, *m*-ZrO_2 seems to deactivate much more rapidly than *t*-ZrO_2 (conversion of α-AL decreases by 15 % after only 2 h of reaction over *m*-ZrO_2, in contrast to a $< 10\%$ decrease in conversion after almost 10 h over *t*-ZrO_2). For both catalysts, the decrease in α-AL conversion was accompanied by a significant increase in the formation of β-AL The β isomer becomes the main product over *m*-ZrO_2 after 6 h of reaction, exceeding EL. Notably, for both catalytic systems, the mixture of products obtained towards the end of the reaction has a ratio α-AL/β-AL ~ 1, suggesting that the two isomeric forms have similar reactivity and the isomerisation processes were quite fast in our experimental conditions, probably reaching the equilibrium. It is evident that the *t*-ZrO_2 exhibited the higher efficiency in terms of both GVL yield and reactants conversion, as opposed to the monoclinic form. Finally, a test was performed feeding a mixture of GVL and ethanol over both *m*- and t- ZrO_2 (see Figure S7 in the SI). In both cases, GVL conversion tends to stabilise at 30% after few hours of time on stream; however, while *t*-ZrO_2 shows significant yield in EP (ca. 20%), demonstrating its ability to foster consecutive reactions on GVL, *m*-ZrO_2 yield EP only in traces. The average molar balances were relatively low in both cases, nonetheless while TGA showed relatively low accumulation of organics over the surface (see Figure S8 in the SI), qualitative gas phase analysis on GC–MS underlined the presence of light hydrocarbons (e.g. butenes), suggesting that ALs play a fundamental role in catalyst deactivation. Finally, the effect of the molar ratio between ethanol and ML in the feed has been investigated in the range of 20:1 and 4:1 (Fig. 6, S9 and S10) by working at 250 °C and 1 s of contact time.

All these tests clearly underline the crucial role of an effective adsorption and activation of ethanol for the promotion of the CTH process and for an efficient dilution of some ML derivatives, such as AL and other coke precursors. Noteworthy, by working with higher ethanol excess, GVL yield values were above 60% for more than four hours of time on stream reaching a maximum of 75% before the deactivation kicks in. Indeed, the deactivation phenomena over both the ZrO_2 polymorphs were strongly delayed but became negligible only in the case of the tetragonal form (Figure S9). On the opposite, the tests performed feeding a mixture with a lower ethanol excess (ML:EtOH = 1:4, Figure S10) immediately led to the selectivity drops of GVL favouring the formation of EL via AL alcoholysis or ML transesterification, however with the already highlighted differences of performances which indicates *t*-ZrO_2 the most suitable and stable materials for the CTH of ML with ethanol in the gas-phase to date.

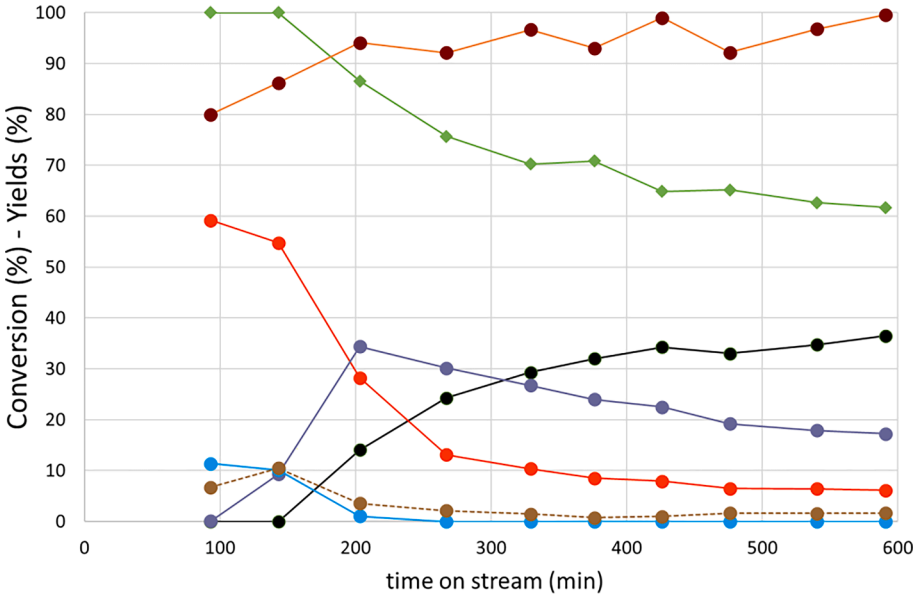

Fig. 5. Catalytic results obtained in α-AL reduction via CTH using EtOH as H-donor over *m*-ZrO_2. Reaction conditions: molar ratio α-AL:EtOH = 1:10, T = 250 °C, τ = 1 s, %mol N_2: α-AL:EtOH = 90.1:0.9:9. Conversion (◆); EL (●); GVL ((●); Ethyl GVL (●); βAL (●); Others (●); Yields sum/ Conversion (● dotted line).

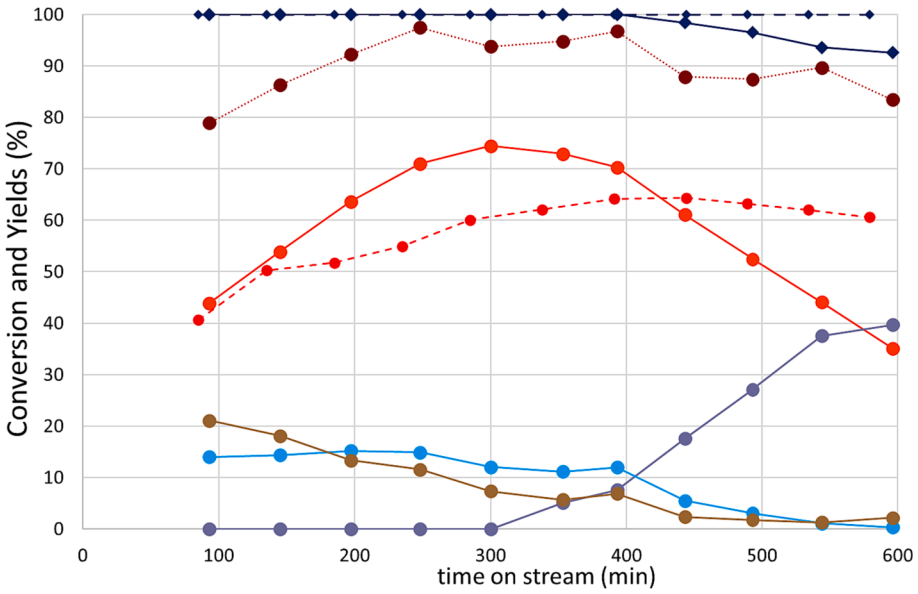

Fig. 6. Catalytic results obtained in ML reduction via CTH using EtOH as H-donor over *m*-ZrO_2. Reaction conditions: molar ratio ML:EtOH = 1:20, T = 250 °C, τ = 1 s, %mol N_2:ML:EtOH = 89.5:0.5:10. Conversion (◆); EL (●); GVL (●); Ethyl GVL (●); βAL (●); Others (●); Yields sum/Conversion (● dotted line). For the sake of comparison, the results obtained over *t*-ZrO_2 are also reported with dashed line in terms of both ML conversion (◆) and GVL yield (●).

3.3. ^1H NMR relaxation results

The relative adsorption strengths of alkyl levulinates (ML and EL, referred also as "reactants"), products (α-AL and GVL) and alcohols (ethanol and the co-produced methanol) were characterised using low-field NMR relaxation measurements, to assess how the interaction of species present during the reaction with the different phases of ZrO_2 impacts the catalytic performance. It is important to note that, in this context, NMR relaxation measurements are not used as an *operando* analytical technique for the characterization of the catalytic reaction under reaction conditions. Rather, it is used as an *ex-situ* analytical tool to characterise surface interactions of the reactants, products and solvents with the catalyst surface. However, it should be noted that although NMR relaxation measurements require the use of liquid phase reactants and products, they are robust in nature and conclusions drawn with regards to surface affinities can also be applied to gas phase species [59-61].

The pores of the ZrO_2 catalysts were filled with the probe liquid of interest and the spin–lattice (T_1) and spin–spin (T_2) relaxation time constants were determined using the inversion recovery and CPMG pulse sequence, respectively (Fig. 1(a) and (b) in the Experimental section). The T_1 and T_2 plots for reactant, products and solvents are shown in the Supporting Information (Table S2, Figures S11- S14).

The ratio of the spin–lattice to spin–spin relaxation time constants (T_1/T_2) has been shown to be an effective measure of the affinity of a molecule of interest and a solid surface [62,63]. In brief, the greater the value of T_1/T_2, the stronger the interaction between the guest molecule and the surface under study. A more detailed explanation of this phenomenon is given in the Supporting Information. Determined T_1/T_2 values are given in Table S2 and can be seen expressed graphically below in Fig. 7.

As shown in Fig. 7, both ethanol and methanol generally interact with the ZrO_2 catalyst surfaces much more strongly than the reactants and products, as indicated by their T_1/T_2 values. Moreover, there is a significant difference in solvent adsorption strength between the two phases of ZrO_2 studied. That is, *t*-ZrO_2 adsorbs both solvents much more strongly than *m*-ZrO_2 despite the greater basicity and acidity of the

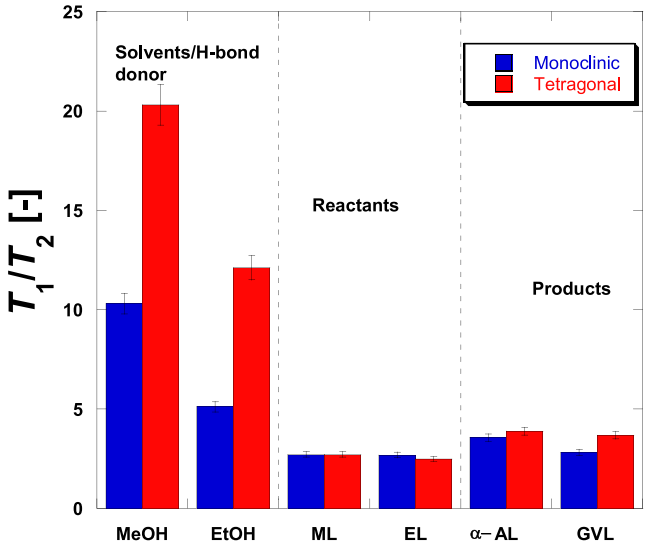

Fig. 7. T_1/T_2 values of the alcohols (MeOH and EtOH), alkyl levulinates (ML and EL) and products (α-AL and GVL) imbibed within the pores of monoclinic and tetragonal ZrO_2 (red and blue columns, respectively). A higher T_1/T_2 value is indicative of a greater strength of surface interaction. The error of all T_1/T_2 values is ± 3 %. (For interpretation of the references to colour in this figure legend, the reader is referred to the web version of this article.)

latter. It is likely that the alcohol solvents interact strongly with surface hydroxyls on the *t*-ZrO_2 surfaces *via* H-bonding as well as interacting with Lewis acid sites, which strength seems to be quite similar in the two polymorphs. The different T_1/T_2 values could also been explained taking into account a complex, extended H-bonding network in which, by working in the liquid phase with the pure alcohols may lead to a favourable, geometrical adsorption of either ethanol or methanol in the case of the tetragonal structure. The catalytic results (as shown in Figs. 3 and 4) have demonstrated that, under continuous conditions, both a

higher GVL yield and enhanced catalyst stability are obtained on *t*-ZrO_2 with respect to *m*-ZrO_2. As EtOH is the H-donor/reducing agent in the CTH reaction, it is plausible to conclude that a greater interaction of the alcohols with ZrO_2 "activates" the alcohol molecules, producing molecules with a greater H-donating ability (likely by weakening the O–H bond during H-bonding with surface hydroxyls) and thereby increasing catalytic activity. The higher interactions of the H-donor species with the *t*-ZrO_2 phase could also explain the catalyst stability data. It is observed that *t*-ZrO_2 phase is much more stable than the *m*-ZrO_2 phase, which is attributed to the larger extent of carbonaceous deposition over the latter phase. In this context, the greater strength of interactions of the alcohols over the *t*-ZrO_2 phase could hence help the overall target process for two reasons: i) effectively enhancing the activation of ethanol toward the CTH processes and ii) promoting a competitive adsorption over specific sites (e.g. Lewis acid sites) which enhance an effective "dilution" of coke precursors (i.e. AL) over the catalyst surface, thus increasing the stability of the *t*-ZrO_2 phase.

The relative adsorption strengths of the alkyl levulinates (ML and EL, $T_1/T_2 \sim 2.7$ for *m*-ZrO_2 and t-ZrO_2) and products (GVL and α-AL, $T_1/T_2 \sim 3.7$ for *m*-ZrO_2 and t-ZrO_2) are statistically similar (see Fig. 7, and Table S2 in the SI), indicating that four liquids have a similar strength of surface interaction regardless of the ZrO_2 phase used. This would suggest that the strength of interaction between the catalytic surface and ML, EL, GVL and α-AL, alone, should not significantly impact the differences in catalytic performance between the two different phases of ZrO_2. Rather, differences in catalytic activity between *m*-ZrO_2 and *t*-ZrO_2 for this reaction, are defined by the interaction between the catalyst and the H-donor. That is, a stronger H-bond between the alcohol solvent and ZrO_2 surface hydroxyls and Lewis acid sites will weaken the alcohol O–H bond, making H more available for CTH. Additionally, a slightly higher T_1/T_2 value of GVL over *t*-ZrO_2 can suggest a stronger interaction of this compound which may lead to the promotion of the experimentally observed consecutive reaction towards EP.

3.4. Computational results

3.4.1. Modelling ZrO_2 clusters

As mentioned in the 'Computational methods' section, the "cluster approach" was used to model the catalytic ZrO_2 nanoparticles in order to analyse the adsorption properties of nanoparticle surface low-coordinated sites and to possibly obtain insights into the different catalytic behaviour of the two ZrO_2 phases. The models were built starting from the unit cells of the monoclinic and the tetragonal crystallographic phases of ZrO_2, as attainable from the Material Project database [64]. The unit cell was then repeated three-dimensionally to obtain a bulk-like structure that was then cut along the most thermodynamically most stable surfaces of the two phases respectively [65]. For *t*-ZrO_2, the catalyst model was built by cutting along the O-terminated (1 0 1) crystallographic planes to expose the thermodynamically most stable surfaces and terminations following the modelling proposed by Puigdollers *et al* [66]. An octahedral nanoparticle (O-np) with $Zr_{19}O_{32}$ stoichiometry was obtained. Instead, for the *m*-ZrO_2, a $Zr_{18}O_{33}$ cluster was built, where the two more extended facets are the thermodynamically most stable (1 1 1) surfaces. The DFT optimized structures of these clusters are reported in Fig. 8.

In carrying out the subsequent adsorption studies, it is important to consider the coordination of the Zr atoms in the cluster models under consideration. In particular, the Zr atoms in the edge of the cluster structures (namely, the 'edge sites') have an average coordination number of 5.1 and 6.0 for *m*-ZrO_2 and *t*-ZrO_2, respectively, which are close to those (5 and 7, respectively) of their most stable exposed surfaces, i.e. (1 1 1) and (1 0 1), respectively. Instead, the 'vertex sites', with lower coordination than edge ones, feature coordination numbers of 4.1 and 4.0 for Zr atoms in *m*-ZrO_2 and *t*-ZrO_2 clusters, respectively. Thus, we can consider the edge sites as the most representative for the adsorption on the catalyst nanoparticles, since they are expected to be much more numerous than the vertex sites in the real catalysts. However, the vertex sites represent the lowest-coordinated sites, thus potentially the most reactive ones.

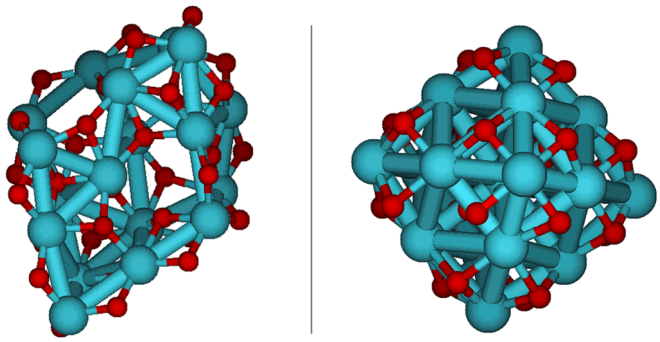

Fig. 8. The $Zr_{18}O_{33}$ and $Zr_{19}O_{32}$ DFT cluster models of m-ZrO_2 (left) and t-ZrO_2 (right) nanoparticles.

3.4.2. Analysis of the strength of Lewis acidic sites: NH_3 adsorption

On the DFT optimised structures, the strength of the acidic and basic sites was evaluated, comparing the results for the two crystalline phases of ZrO_2. In particular, the acidic sites are studied by the adsorption of NH_3 and compared with TPD experiments reported above [66,67]. Our comparison of adsorption energies of NH_3 on tetragonal and monoclinic zirconia indicates that the adsorption energies range is similar for both phases for the edge sites, suggesting overall similar adsorption properties, in line with experimental TPD evidence. In particular, for the strongest adsorption site on *t*-ZrO_2, which is an edge site, the adsorption energy is −28.9 kcal/mol, while for *m*-ZrO_2 is −29.2 kcal/mol (on a vertex site) with corresponding DFT optimised structures reported in Fig. 9. Also, the Zr-N distance is similar in these two structures, with a value of 2.40 Å for the tetragonal phase and 2.42 Å for the monoclinic one. As shown in Table S2, the most representative sites for *m*-ZrO_2 and *t*-ZrO_2 nanoparticles, i.e. the edge sites, feature comparable adsorption energies, while for vertex sites there is stronger adsorption on *m*-ZrO_2 than *t*-ZrO_2. This would suggest that the relatively small difference in the TPD peak temperature (showed in Fig. 2) can be interpreted as an indication of stronger acidic sites on the *m*-ZrO_2 with respect to *t*-ZrO_2, which is related to the lowest-coordinated sites of the nanoparticle catalysts.

3.4.3. Analysis of the strength of Lewis basic sites: CO_2 adsorption

In the CTH, the amphoteric character of the catalyst is an important feature as it promotes the capacity of the alcohol to donate a proton by generating an alkoxide [21]. The basicity was studied with the adsorption of CO_2, that on metal oxides typically leads to carbonate adsorbed species. Our DFT investigations indicated, in fact, that adsorbing the C

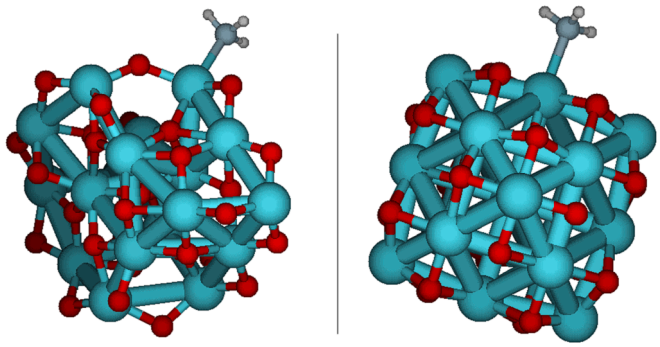

Fig. 9. Adsorption of NH_3 on *m*-ZrO_2 (left) and *t*-ZrO_2 (right) on the site with the largest adsorption energies.

atom of CO_2 on top oxygen basic sites of ZrO_2 one of the oxygens of CO_2 always tends to bind to a surface Zr atom.

The interaction with basic sites implies a donation to the CO_2 antibonding π* orbital and a consequent elongation of the C-O bond along with deviation from the linearity of the free molecule. The more the bond is elongated and the bond angle is deviated from 180°, the more the donation is significant, therefore, the more basic the site [68-70]. The adsorption energy, inevitably associated to the formation of carbonate adsorbed species, is not the best parameter for the characterisation of the strength of surface basic sites. Indeed, the adsorption energy is associated not just to the interaction between the basic surface site and the acid adsorbate molecule but also to those with other atoms adjacent to the surface atomic site. For these reasons, the strength of the basic site can be analysed by looking at the geometrical parameters (bond angle and bond lengths) of the distorted adsorbed CO_2 molecule incorporated in the carbonate adsorbed species (Fig. 10). In our DFT investigations, we observed that the carbonate adsorbed species are preferentially formed by interaction with Zr vertex sites on *t*-ZrO_2, while on *m*-ZrO_2 they have been found on both vertex and edge sites. Among all stable absorbed species characterised in this work, a consistent trend that differentiates the two crystalline phases of zirconia can be found (see Table S4 in the SI): the CO_2 bends more on *m*-ZrO_2 than on *t*-ZrO_2 and one of the two C-O bonds of CO_2 gets elongated in the case of monoclinic ZrO_2. Considering the two lowest energy structures of adsorbed CO_2 on the two phases, the CO_2 bends with an angle of 122° and 132° and the C-O bond elongates to 1.38 Å and 1.30 Å on *m*-ZrO_2 and *t*-ZrO_2, respectively. This indicates a greater donation of electrons to CO_2 and therefore a stronger basic surface site for the monoclinic zirconia compared to the tetragonal one, in agreement with the experimental TPD-CO_2 analysis.

3.4.4. *AL adsorption and catalyst deactivation*

To understand the faster deactivation of *m*-ZrO_2 when compared to *t*-ZrO_2 in the CTH of ML to GVL, we focused the computational study on the adsorption of α-AL for the two phases. Indeed, one of the possible reasons for the different reactivities of the two crystalline phases is the deactivation of the catalyst by formation of heavy products that block the catalytically active surface sites. It is known that the oligomerisation of AL easily proceeds over either basic sites or catalyst characterised by strong acidity [58,71]. One possibility is the ring-opening polymerization of α-AL in the presence of a suitable nucleophile (e.g. an alkoxide) [72] promoted by the activation of AL carbonyl group over Lewis acid sites, forming polyesters. Notably, we found that the adsorption mode with the α-AL carbonyl oxygen over the Lewis acid sites (with Zr-O (α-AL) bond distance ranging from 2.26 to 2.32 Å, see Fig. 11) is the most favourable on both *m*-ZrO_2 and *t*-ZrO_2. A wide range of adsorption energies, from −17.8 to −32.7 kcal/mol, have been obtained for the vertex-type sites (see Table S5 in the SI). Instead, comparing the most stable adsorptions of α-AL on the edge sites for the two crystalline phases, a similar adsorption energy is found, in the range between −20.1 and −22.7 kcal/mol. Since the edge sites are certainly much more numerous than vertices on the exposed surface of nanoparticles, the similar adsorption energies found for these sites on the two crystalline phases agree with the NMR results that indicated similar adsorption strengths for α-AL on *m*-ZrO_2 and *t*-ZrO_2 (see Fig. 7).

However, considering the α-AL adsorption on the Zr vertex sites we found a much stronger adsorption on the monoclinic phase (−32.7 kcal/mol) than on the tetragonal one (-18.4 kcal/mol). Since these adsorption sites are expected to be present in a much smaller extent than edge sites on the real nanoparticles, such difference in adsorption energies should not significantly affect the average adsorption energies of α-AL on *m*-ZrO_2 and *t*-ZrO_2. At the same time, these sites are associated to the lowest-coordinated and most reactive Zr atoms, thus the difference in adsorption energy on these sites between the two phases might have a significant impact on their overall reactivity.

Indeed, the stronger the Zr-O(α-AL) surface interaction of α-AL on *m*-ZrO_2 can lead to a faster deactivation of the catalyst with respect to *t*-ZrO_2, since the longer residence time on the most reactive sites would correspond to likelier formation of oligomers, thereby promoting surface deactivation. However, the longer residence time that, accordingly to DFT computations, we could clearly expect on the lowest-coordinated Zr sites, should be accompanied by the contemporary presence of activated AL surface species. The activation of α-AL species on ZrO_2 surfaces could actually occur if the Lewis basic sites (i.e. surface oxygens) are able to deprotonate the α-AL, following a base-assisted dimerization/polymerization process [71,73] Most likely, this deprotonation will involve the most acidic H of α-AL, i.e. one of the two hydrogens in alpha position with respect to the AL carbonyl (namely H_α). As shown in Fig. 11, the shortest distances between the acidic H_α and ZrO_2 surface oxygen, i.e. H_α-*O(ZrO$_2$)*, are found to be significantly shorter in *m*-ZrO_2 than in *t*-ZrO_2, being in the ranges 2.32–2.43 Å and 2.57–2.72 Å, respectively. This has to be mainly ascribed to the different exposition of surface oxygens on the two phase and to the adsorption mode of α-AL via the carbonyl oxygen, which directs the C-H_α bonds towards the surface basic sites. Notably, the difference in H_α-*O(ZrO$_2$)* distance between the two phases is more evident for the most numerous edge surface sites (ca. 0.40 Å) than for the vertices (ca. 0.14 Å). This outcome strongly suggests that the acidic H_α are closer to the basic surface sites on the *m*-ZrO_2 than

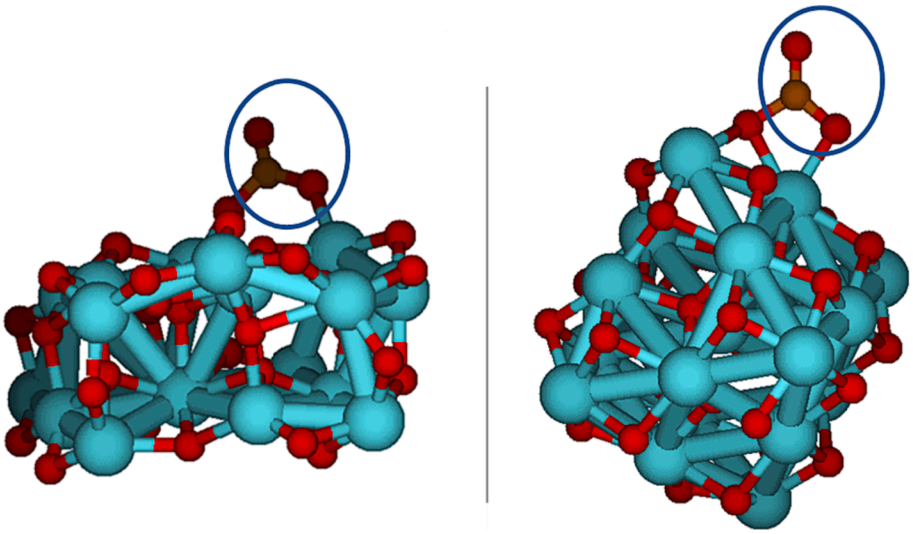

Fig. 10. Adsorption of CO_2 on *m*-ZrO_2 (left) and *t*-ZrO_2 (right).

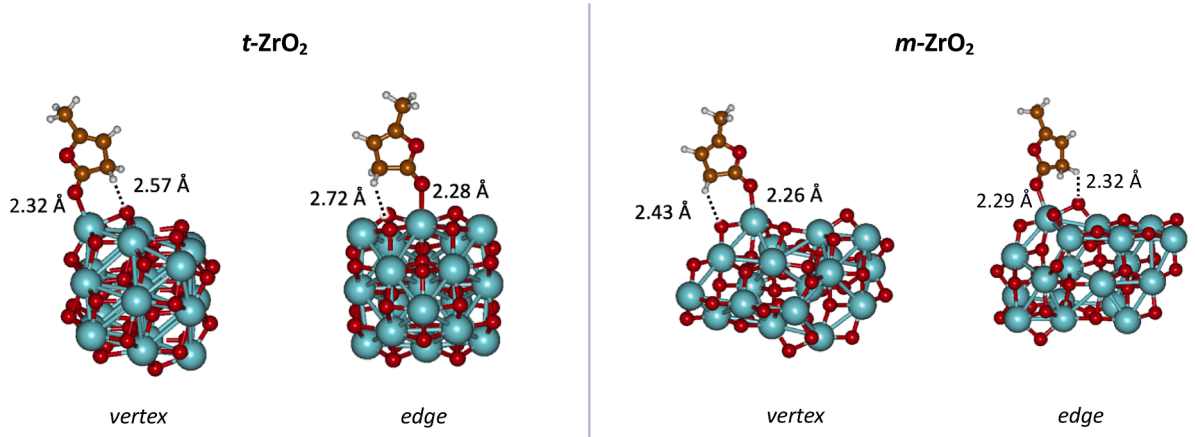

Fig. 11. Adsorption of α-AL on *t*-ZrO_2 (left) and *m*-ZrO_2 (right) on the most stable adsorption sites for both the vertex- and edge-type sites. Zr-O(α-AL) distance (red stick) and H_α-O(ZrO_2) distance (black dotted lines) are reported in Å. (For interpretation of the references to colour in this figure legend, the reader is referred to the web version of this article.)

on the *t*-ZrO_2. These results, combined with the different strength of the basic sites described above, clearly indicate that the formation of oligomers and consequent deactivation of the catalyst is more likely on *m*-ZrO_2 than *t*-ZrO_2.

4. Conclusions

In conclusion, the monoclinic and tetragonal phases of zirconia were tested in the continuous-flow, gas-phase, catalytic transfer hydrogenation (CTH) of ML with ethanol toward GVL and other compounds of interest (i.e. ethyl-GVL and ethyl pentenoates). The effect of temperature and reagent molar ratio on products distribution have been investigated and a reaction intermediate (α-AL) and a product (GVL) have been fed in order to better understand the reaction pathway and underline the different behaviours of these two different crystalline phases on the target reaction. The observed experimental results were linked not only with thermogravimetric analysis and DRIFT spectroscopy but also with both NMR spectroscopy and DFT calculations in order to assess the structure–activity relationship. The obtained results clearly show an improved efficiency for *t*-ZrO_2 in ethanol adsorption and activation, which lead to an enhanced CTH process and an efficient dilution over the catalytic surface of the AL, the main responsible of carbonaceous species deposition via ring-opening oligomerisation. These phenomena allow to improve catalyst lifetime and GVL yield (between 60 and 70%) over the time on stream. Conversely, the *m*-ZrO_2 shows faster deactivation trends, due to the faster accumulation of heavy compounds over the catalytic surface, as consequence of the higher Lewis acidity and basicity of this crystalline phase (proved with both TPD experiments and DFT computations) which led to stronger interaction with the intermediate AL. Interestingly, by increasing the molar excess between ethanol and ML to 20, both systems show improved stability with an almost negligible deactivation showed by *t*-ZrO_2. However, in these conditions, while the tetragonal is able to foster consecutive reaction over GVL, promoting the formation of ethyl pentenoates, the *m*-ZrO_2 shows the higher GVL yield of 75% after 6 h of time on stream. These results may open new perspective toward catalyst optimisation for an efficient and actually sustainable alkyl levulinates reduction toward GVL and related compounds.

CRediT authorship contribution statement

Riccardo Bacchiocchi: Investigation, Writing – original draft. **Alessia Ventimiglia:** Investigation, Data curation, Writing – original draft. **Andrea Canciani:** Investigation, Data curation. **Giorgia Peroni:** Investigation, Visualization. **Tommaso Tabanelli:** Investigation, Conceptualization, Supervision, Writing – review & editing. **Stefania Albonetti:** Conceptualization, Supervision. **Nikolaos Dimitratos:** Conceptualization, Writing – review & editing. **Ivan Rivalta:** Conceptualization, Supervision, Writing – review & editing. **Shima Zainal:** Investigation, Writing – original draft. **Luke Forster:** Investigation, Conceptualization. **Carmine D'Agostino:** Conceptualization, Supervision. **Fabrizio Cavani:** Funding acquisition, Writing – review & editing.

Declaration of Competing Interest

The authors declare that they have no known competing financial interests or personal relationships that could have appeared to influence the work reported in this paper.

Data availability

Data will be made available on request.

Acknowledgements

The authors are grateful to Italian Ministero dell'Università e della Ricerca for the financial support provided through the PRIN 2020 LEVANTE project "LEvulinic acid Valorization through Advanced Novel Technologies" (Progetti di Ricerca di Rilevante Interesse Nazionale-Bando 2020, 2020CZCJN7).

L.F. and C.D. would like to acknowledge the EPSRC (EP/V026089/1) for supporting their research activities.

Appendix A. Supplementary data

Supplementary data to this article can be found online at https://doi.org/10.1016/j.jcat.2023.115177.

References

[1] F.W. Lichtenthaler, Carbohydrates as Organic Raw Materials, Ullmann's Encyclopedia of Industrial, Chemistry 6 (2010) 584.
[2] S. Solomon, D. Qin, M. Manning, Z. Chen, M. Marquism, K.B. Averyt, IPCC. Climate change 2007: the physical science basis. Contribution of working group 1 to the

fourth assessment report of the intergovernmental panel on climate change. Cambridge, United Kingdom and New York, NY, USA: Cambridge University Press.
[3] B. Metz, O. Davidson, P. Bosch, R. Dave, L.A. Meyer, IPCC. Climate change 2007: mitigation. Contribution of working group 3 to the fourth assessment report of the intergovernmental panel on climate change. Cambridge, United Kingdom and New York, USA: Cambridge University Press.
[4] A.T. Ubando, C.B. Felix, W.-H. Chen, Biorefineries in circular bioeconomy: A comprehensive review, Bioresour. Technol. 299 (2020), 122585.
[5] T. Werpy, G. Petersen, Top value added chemicals from biomass: volume 1 results of screening for potential candidates from sugars and synthesis gas, U.S. Department of Energy, Washington DC, 2004.
[6] D.W. Rackemann, W.O. Doherty, The Conversion of Lignocellulosics to Levulinic Acid, Biofuels, Bioprod. Biorefin. 5 (2) (2011) 198–214.
[7] Y.-B. Huang, T. Yang, Y.-T. Lin, Y.-Z. Zhu, L.-C. Lia, H. Pan, Facile and high-yield synthesis of methyl levulinate from cellulose, Green Chem. 20 (2018) 1323–1334.
[8] A.M. Raspolli Galletti, C. Antonetti, S. Fulignati, D. Licursi, Direct Alcoholysis of Carbohydrate Precursors and Real Cellulosic Biomasses to Alkyl Levulinates: A Critical Review, Catalysts 10 (2020) 1221.
[9] M. Grilc, B. Likozar, Levulinic acid hydrodeoxygenation, decarboxylation and oligmerization over NiMo/Al2O3 catalyst to bio-based value-added chemicals: Modelling of mass transfer, thermodynamics and micro-kinetics, Chem. Eng. J. 330 (2017) 383–397.
[10] A. Chatzidimitriou, J.Q. Bond, Oxidation of levulinic acid for the production of maleic anhydride: breathing new life into biochemicals, Green Chem. 17 (2015) 4367–4376.
[11] Y. Shao, S. Ba, K. Sun, G. Gao, M. Fan, J. Wang, H. Fan, L. Zhang, X. Hu, Selective production of γ-valerolactone or 1,4-pentanediol from levulinic acid/esters over Co-based catalyst: Importance of the synergy of hydrogenation sites and acidic sites, Chem. Eng. J. 429 (2022), 132433.
[12] A. Bellè, T. Tabanelli, G. Fiorani, A. Perosa, F. Cavani, M. Selva, A Multiphase Protocol for Selective Hydrogenation and Reductive Amination of Levulinic Acid with Integrated Catalyst Recovery, ChemSusChem 12 (14) (2019) 3343–3354.
[13] D. Carnevali, M.G. Rigamonti, T. Tabanelli, G.S. Patience, F. Cavani, Levulinic acid upgrade to succinic acid with hydrogen peroxide, Appl. Catal. A 563 (2018) 98–104.
[14] K. Yan, C. Jarvis, J. Gu, Y. Yan, Production and Catalytic Transformation of Levulinic Acid: A Platform for Speciality Chemicals and Fuels, Renew. Sustain. Energy Rev. 51 (2015) 986–997.
[15] J. Zhang, S. Wu, B. Li, H. Zhang, Advances in the Catalytic Production of Valuable Levulinic Acid Derivatives, ChemCatChem 4 (2012) 1230–1237.
[16] U. Omoruyi, S. Page, J. Hallett, P.W. Miller, Homogeneous Catalysed Reactions of Levulinic Acid: To γ-Valerolactone and Beyond, ChemSusChem 9 (2016) 2037–2047.
[17] A.M.R. Galletti, C. Antonetti, V. De Luise, M. Martinelli, A sustainable process for the production of γ-valerolactone by hydrogenation of biomass-derived levulinic acid, Green Chem. 14 (2012) 688–694.
[18] K. Mustafin, F. Cárdenas-Lizana, M.A. Keane, Continuous Gas Phase Catalytic Transformation of Levulinic Acid to γ-Valerolactone over Supported Au Catalysts, J. Chem. Technol. Biotechnol. 92 (9) (2017) 2221–2228.
[19] D. Sun, A. Ohkubo, K. Asami, T. Katori, Y. Yamada, S. Sato, Vapor-phase hydrogenation of levulinic acid and methyl levulinate to γ-valerolactone over non-noble metal-based catalysts, Molecular, Catalysis 437 (2017) 105–113.
[20] G. Grillo, M. Manzoli, F. Bucciol, S. Tabasso, T. Tabanelli, F. Cavani, G. Cravotto, Hydrogenation of Levulinic Acid to γ-Valerolactone via Green Microwave-Assisted Reactions Either in Continuous Flow or Solvent-Free Batch Processes, Ind. Eng. Chem. Res. 60 (46) (2021) 16756–16768.
[21] T. Komanoya, K. Nakajima, M. Kitano, M. Hara, Synergistic Catalysis by Lewis Acid and Base Sites on ZrO_2 for Meerwein- Ponndorf-Verley Reduction, J. Phys. Chem. C. 119 (47) (2015) 26540–26546.
[22] T. Tabanelli, Unrevealing the hidden link between sustainable alkylation and hydrogen transfer processes with alcohols, Curr. Opin. Green Sustain. Chem. 29 (2021), 100449.
[23] M.S. Gyngazova, L. Grazia, A. Lolli, G. Innocenti, T. Tabanelli, M. Mella, S. Albonetti, F. Cavani, Mechanistic insights into the catalytic transfer hydrogenation of furfural with methanol and alkaline earth oxides, J. Catal. 372 (2019) 61–73.
[24] L. Grazia, D. Bonincontro, A. Lolli, T. Tabanelli, C. Lucarelli, S. Albonetti, F. Cavani, Exploiting H-transfer as a tool for the catalytic reduction of bio-based building blocks: the gas-phase production of 2-methylfuran using a $FeVO_4$ catalyst, Green Chem. 19 (2017) 4412–4422.
[25] S. Rojas-Buzo, P. Garcia-Garcia, A. Corma, Catalytic transfer hydrogenation of biomass-derived carbonyls over hafnium- based metal–organic frameworks, ChemSusChem 11 (2018) 432–438.
[26] D. Scholz, C. Aelli, I. Hermans, Catalytic transfer hydrogenation/hydrogenolysis for reductive upgrading of furfural and 5-(hydroxymethyl)furfural, ChemSusChem 7 (2014) 268–275.
[27] B. Garcia, J. Moreno, J.A. Iglesias, J. Melero, G. Morales, Transformation of glucose into sorbitol on raney nickel catalysts in the absence of molecular hydrogen: sugar disproportionation vs catalytic hydrogen transfer, Top. Catal. 62 (2019) 570–578.
[28] M. Chia, J.A. Dumesic, Liquid-Phase Catalytic Transfer Hydrogenation and Cyclization of Levulinic Acid and Its Esters to γ- Valerolactone over Metal Oxide Catalysts, Chem. Commun. 47 (2011) 12233–12235.
[29] K. Maresz, A. Ciemi, J. Mrowiec-Biało, Selective Reduction of Ketones and Aldehydes in Continuous-Flow Microreactor: Kinetic Studies, Catalysts 8 (5) (2018) 221.
[30] X. Tang, L. Hu, Y. Sun, G. Zhao, W. Hao, L. Lin, Conversion of Biomass-Derived Ethyl Levulinate into γ-Valerolactone via Hydrogen Transfer from Supercritical Ethanol over a ZrO_2 Catalyst, RSC Adv. 3 (26) (2013) 10277.
[31] Y. Xie, F. Li, J. Wang, R. Wang, H. Wang, X. Liu, Y. Xia, Catalytic transfer hydrogenation of ethyl levulinate to γ-valerolactone over a novel porous Zirconium trimetaphosphate, Molecular, Catalysis 442 (2017) 107–114.
[32] J. Lai, S. Zhou, X. Liu, Y. Yang, J. Lei, Q. Xu, D. Yin, Catalytic Transfer Hydrogenation of Biomass-Derived Ethyl Levulinate into Gamma-Valerolactone Over Graphene Oxide-Supported Zirconia Catalysts, Catal. Lett. 149 (2019) 2749–2757.
[33] P.B. Vásquez, T. Tabanelli, E. Monti, S. Albonetti, D. Bonincontro, N. Dimitratos, F. Cavani, Gas-Phase Catalytic Transfer Hydrogenation of Methyl Levulinate with Ethanol over ZrO_2, ACS Sustain. Chem. Eng. 7 (9) (2019) 8317–8330.
[34] T. Tabanelli, E. Paone, P. Blair Vasquez, R. Pietropaolo, F. Cavani, F. Mauriello, Transfer Hydrogenation of Methyl and Ethyl Levulinate Promoted by a ZrO_2 Catalyst: Comparison of Batch vs Continuous Gas-Flow Conditions, ACS Sustain Chem. Eng. 7 (2019) 9937–9947.
[35] S. Shukla, S. Seal, Mechanisms of Room Temperature Metastable Tetragonal Phase Stabilisation in Zirconia, Int. Mater. Rev. 50 (2005) 45–64.
[36] E.M. Albuquerque, L.E.P. Borges, M.A. Fraga, C. Sievers, Relationship between Acid-Base Properties and the Activity of ZrO_2-Based Catalysts for the Cannizzaro Reaction of Pyruvaldehyde to Lactic Acid, ChemCatChem 9 (2017) 2675–2683.
[37] G.K. Chuah, S. Jaenicke, S.A. Cheong, K.S. Chan, The influence of preparation conditions on the surface area of zirconia, Appl. Catal. A 145 (1–2) (1996) 267–284.
[38] E. Fukushima, S.W. Roeder, Experimental pulse NMR, a nuts and bolts approach, CRC Press, 1981.
[39] H.Y. Carr, E.M. Purcell, Effects of Diffusion on Free Precession in Nuclear Magnetic Resonance Experiments, Phys. Rev. 94 (1954) 630.
[40] M.J. Gilkey, B. Xu, Heterogeneous Catalytic Transfer Hydrogenation as an Effective Pathway in Biomass Upgrading, ACS Catal. 6 (3) (2016) 1420–1436.
[41] C. Lahousse, A. Aboulayt, F. Maugé, J. Bachelier, J.C. Lavalley, Acidic and basic properties of zirconia-alumina and zirconia-titania mixed oxides, J. Mol. Catal. 84 (1993) 283–297.
[42] A.D. Becke, Density-functional thermochemistry. III. The role of exact exchange, J. Chem. Phys. 98 (1993) 5648–5652, https://doi.org/10.1063/1.464913.
[43] Gaussian 16, Revision C.01, M. J. Frisch; G. W. Trucks, H. B. Schlegel, G. E. Scuseria, M. A. Robb, J. R. Cheeseman, G. Scalmani, V. Barone, G. A. Petersson, H. Nakatsuji, X. Li, M. Caricato, A. V. Marenich, J. Bloino, B. G. Janesko, R. Gomperts, B. Mennucci, H. P. Hratchian, J. V. Ortiz, A. F. Izmaylov, J. L. Sonnenberg, D. Williams-Young, F. Ding, F. Lipparini, F. Egidi, J. Goings, B. Peng, A. Petrone, T. Henderson, D. Ranasinghe, V. G. Zakrzewski, J. Gao, N. Rega, G. Zheng, W. Liang, M. Hada, M. Ehara, K. Toyota, R. Fukuda, J. Hasegawa, M. Ishida, T. Nakajima, Y. Honda, O. Kitao, H. Nakai, T. Vreven, K. Throssell, J. A. Montgomery, Jr., J. E. Peralta, F. Ogliaro, M. J. Bearpark, J. J. Heyd, E. N. Brothers, K. N. Kudin, V. N. Staroverov, T. A. Keith, R. Kobayashi, J. Normand, K. Raghavachari, A. P. Rendell, J. C. Burant, S. S. Iyengar, J. Tomasi, M. Cossi, J. M. Millam, M. Klene, C. Adamo, R. Cammi, J. W. Ochterski, R. L. Martin, K. Morokuma, O. Farkas, J. B. Foresman, and D. J. Fox, Gaussian, Inc., Wallingford CT, 2016.
[44] A. D. McLean, G. S. Chandler, Contracted Gaussian-basis sets for molecular calculations. 1. 2nd row atoms, Z=11-18, J. Chem. Phys. 72 (1980) 5639-48.
[45] K. Raghavachari, J.S. Binkley, R. Seeger, J.A. Pople, Self-Consistent Molecular Orbital Methods. 20. Basis set for correlated wave-functions, J. Chem. Phys. 72 (1980) 650–654.
[46] L.A. Curtiss, M.P. McGrath, J.-P. Blaudeau, N.E. Davis, R.C. Binning Jr., L. Radom, Extension of Gaussian-2 theory to molecules containing third-row atoms Ga-Kr, J. Chem. Phys. 103 (1995) 6104–6113.
[47] M.P. McGrath, L. Radom, Extension of Gaussian-1 (G1) theory to bromine-containing molecules, J. Chem. Phys. 94 (1991) 511–516.
[48] R.C. Binning, L.A. Curtiss, Compact contracted basis-sets for 3rd-row atoms – GA-KR, J. Comp. Chem. 11 (1990) 1206–1216.
[49] D. Andrae, U. Häußermann, M. Dolg, H. Stoll, H. Preuß, Energy-adjusted ab initio pseudopotentials for the second and third row transition elements, Theor. Chim. Acta 77 (1990) 123–141.
[50] S.F. Boys, F. Bernardi, Calculation of Small Molecular Interactions by Differences of Separate Total Energies - Some Procedures with Reduced Errors, Mol. Phys. 19 (1970) 553, https://doi.org/10.1080/00268977000101561.
[51] S. Simon, M. Duran, J.J. Dannenberg, How does basis set superposition error change the potential surfaces for hydrogen bonded dimers? J. Chem. Phys. 105 (1996) 11024–11031.
[52] L. Weizhen, H. Huang, H. Li Wei Zhang, H. Liu, Langmuir, Facile Synthesis of Pure Monoclinic and Tetragonal Zirconia Nanoparticles and Their Phase Effects on the Behavior of Supported Molybdena Catalysts for Methanol-Selective Oxidation, Langmuir 24 (15) (2008) 8358–8366.
[53] D. Simon, B. Taylor, Overcoming the deleterious effect of hafnium in tungsten–zirconia catalysts: The use of doping and thermal treatments, J. Catal. 262 (2009) 127–133.
[54] H.-K. Min, Y.W. Kim, C. Kim, I.A.M. Ibrahim, J.W. Han, Y.-W. Suh, K.-D. Jung, M. B. Park, C.-H. Shin, Phase transformation of ZrO_2 by Si incorporation and catalytic activity for isopropyl alcohol dehydration and dehydrogenation, Chem. Eng. J. 428 (2022), 131766.
[55] G. Busca, The Surface Acidity of Solid Oxides and Its Characterization by IR Spectroscopic Methods. An Attempt at Systematization, Phys. Chem. Chem. Phys. 1 (5) (1999) 723–736.
[56] L. Oliviero, A. Vimont, J.C. Lavalley, F. Romero Sarria, M. Gaillard, F. Maugé, 2,6-Dimethylpyridine as a Probe of the Strength of Brønsted Acid Sites: Study on

Zeolites. Application to Alumina, Phys. Chem. Chem. Phys. 7 (8) (2005) 1861–1869.
[57] P. J. Fagan, C. J. Brandenburg. Cis-3,5-disubstituted-dihydro-furan-2ones and the preparation and use thereof. WO2005/014565 A2.
[58] D. Sun, Y. Takahashi, Y. Yamada, S. Sato, Efficient formation of angelica lactones in a vapor-phase conversion of levulinic acid, Appl. Catal. A Gen. 526 (2016) 62–69.
[59] K. Ralphs, C. D'Agostino, R. Burch, S. Chansai, L.F. Gladden, C. Hardacre, S. L. James, J. Mitchel, S.F.R. Taylor, Assessing the surface modifications following the mechanochemical preparation of a Ag/Al_2O_3 selective catalytic reduction catalyst, Catal. Sci. Technol. 4 (2014) 531–539.
[60] C. D'Agostino, S. Chansai, I. Bush, C. Gao, M.D. Mantle, C. Hardacre, S.L. James, L. F. Gladden, Assessing the effect of reducing agents on the selective catalytic reduction of NOx over Ag/Al_2O_3 catalysts, Catal. Sci. Technol. 6 (2016) 1661–1666.
[61] M.H. Haider, C. D'Agostino, N.F. Dummer, M.D. Mantle, L.F. Gladden, D. W. Knight, D.J. Willock, D.J. Morgan, S.H. Taylor, G.J. Hutchings, The Effect of Grafting Zirconia and Ceria onto Alumina as a Support for Silicotungstic Acid for the Catalytic Dehydration of Glycerol to Acrolein, Chem. A Eur. J. 20 (2014) 1743–1752.
[62] C. D'Agostino, J. Mitchell, M.D. Mantle, L.F. Gladden, Interpretation of NMR Relaxation as a Tool for Characterising the Adsorption Strength of Liquids inside Porous Materials, Chem.-A Eur. J. 20 (2014) 13009–13015.
[63] G. Di Carmine, L. Forster, S. Wang, C. Parlett, A. Carlone, C. D'Agostino, NMR relaxation time measurements of solvent effects in an organo-catalysed asymmetric aldol reaction over silica SBA-15 supported proline, React. Chem. Eng. 7 (2) (2022) 269–274.
[64] A. Jain, S.P. Ong, G. Hautier, W. Chen, W.D. Richards, S. Dacek, S. Cholia, D. Gunter, D. Skinner, G. Ceder, K.A. Persson, The Materials Project: A Materials Genome Approach to Accelerating Materials Innovation APL Materials 1(1) (2013) 011002.
[65] C. Ricca, A. Ringuedé, M. Cassir, C. Adamo, F. Labat, A comprehensive DFT investigation of bulk and low-index surfaces of ZrO_2 polymorphs, J. Comput. Chem. 36 (2015) 9–21.
[66] A.R. Puigdollers, F. Illas, G. Pacchioni, Structure and Properties of Zirconia Nanoparticles from Density Functional Theory Calculations, J. Phys. Chem. C 120 (8) (2016) 4392–4402.
[67] F. Maleki, G. Pacchioni, Characterization of Acid and Basic Sites on Zirconia Surfaces and Nanoparticles by Adsorbed Probe Molecules: A Theoretical Study, Top. Catal. 63 (2020) 1717–1730.
[68] K. Bhattacharyya, A. Danon, B.K. Vijayan, K.A. Gray, P.C. Stair, E. Weitz, Role of the Surface Lewis Acid and Base Sites in the Adsorption of CO_2 on Titania Nanotubes and Platinized Titania Nanotubes: An in Situ FT-IR Study, J. Phys. Chem. C 117 (24) (2013) 12661–12678.
[69] H.-Y.-T. Chen, S. Tosoni, G. Pacchioni, A DFT Study of the Acid-Base Properties of Anatase TiO_2 and Tetragonal ZrO_2 by Adsorption of CO and CO_2 Probe Molecules, Surf. Sci. 652 (2016) 163–171.
[70] S. Kouva, J. Andersin, K. Honkala, J. Lehtonen, L. Leffertsac, J. Kanervo, Water and carbon oxides on monoclinic zirconia: Experimental and computational insights, Phys. Chem. Chem. Phys. 16 (2014) 20650–20664.
[71] M. Mascal, S. Dutta, I. Gandarias, Hydrodeoxygenation of the Angelica Lactone Dimer, a Cellulose-Based Feedstock: Simple, High-Yield Synthesis of Branched C7–C10 Gasoline-like Hydrocarbons, Angew. Chem. Int. Ed. 53 (2014) 1854–1857.
[72] T. Chen, Z. Qin, Y. Qi, T. Deng, X. Ge, J. Wang, X. Hou, Degradable Polymers from Ring-Opening Polymerization of α-Angelica Lactone, a Five-Membered Unsaturated Lactone, Polym. Chem. 2 (5) (2011) 1190–1194.
[73] X.-J. Wang, M. Hong, Lewis-Pair-Mediated Selective Dimerization and Polymerization of Lignocellulose-Based b-Angelica Lactone into Biofuel and Acrylic Bioplastic, Angew. Chem. 132 (2020) 2686–2690.